Fusion Engineering and Design 197 (2023) 114030

Contents lists available at ScienceDirect

Fusion Engineering and Design

journal homepage: www.elsevier.com/locate/fusengdes

Atomistic insights into the influence of hydrogen on crack propagation in tungsten

Jun Shi [a,b], Bingchen Li [b,c], Lei Li [b,c], Yifan Liu [b,c], Xinyue Fan [b,c], Qing Peng [d,e,f], Linyun Liang [b,c,*], Shuo Jin [b,c,*], Guang-Hong Lu [b,c]

[a] School of Materials Science and Engineering, Beihang University, Beijing, 100191, China
[b] Beijing Key Laboratory of Advanced Nuclear Materials and Physics, Beihang University, Beijing, 100191, China
[c] School of Physics, Beihang University, Beijing, 100191, China
[d] State Key Laboratory of Nonlinear Mechanics, Institute of Mechanics, Chinese Academy of Sciences, Beijing, 100190, China
[e] School of Engineering Sciences, University of Chinese Academy of Sciences, Beijing, 100049, China
[f] Guangdong Aerospace Research Academy, Guangzhou, 511458, China

ARTICLE INFO

Keywords:
Molecular dynamics simulation
Hydrogen
Crack propagation
Plasma-facing materials
Tungsten

ABSTRACT

Tungsten (W) is regarded as a viable choice for plasma-facing materials in nuclear fusion reactors. However, its mechanical properties are significantly degraded by hydrogen (H) atoms during irradiation, of which the mechanism is still elusive. In this study, we conduct molecular dynamics (MD) simulations to study the impact of H atoms on the propagation of a crack in single crystal W. The results show that the propagation rate of the crack slows down with increasing temperature. This is due to the enhanced plastic deformation, leading to blunting of the crack tip. A pre-existing crack in W is then considered at various temperatures and uniaxial applied tensile strain conditions. The propagation rate of the crack decreases with the increase of the applied tensile strain rate. This phenomenon occurs due to the relaxation of the stress around the crack tip following the emission of the dislocation at high strain rates. After introducing H atoms, it can be observed that at low temperatures, H impedes the propagation of the crack, while at high temperatures, H promotes it. This is primarily due to the formation of voids at the slip traces of dislocations and the reduction in surface energy. Additionally, the crack tip becomes blunted and its propagation rate decreases with increasing strain rate. These results indicate that providing sufficient time for H atoms to migrate is a key factor affecting the mechanical properties of W. The current results provide valuable insights into understanding the interaction mechanism of a crack and H atoms in W.

1. Introduction

Nuclear fusion energy has the potential to offer an unlimited supply of sustainable sources of energy to satisfy the demands of the expanding global population. The materials used in the nuclear fusion reactor must be able to withstand extreme operating conditions. Tungsten (W) has gained recognition as a viable choice for plasma-facing materials (PFMs) in nuclear fusion reactors [1] because of its high thermal conductivity [2], relatively low sputtering yield [3,4], and low hydrogen (H) isotope retention [5]. PFMs experience severe conditions during their service including high temperature, high-energy neutron irradiation [6], as well as exposure to H and helium (He) plasma irradiation [7,8]. These conditions induce a significant amount of displacement-damaged defects, including vacancies and self-interstitial atoms (SIAs). Formed point defects subsequently undergo evolution, aggregating into clusters including voids and dislocations. H and its isotopes, owing to their small sizes, escape from the plasma and can easily diffuse into PFMs. The interaction of the irradiation defects with H and its isotopes causes the brittleness of PFMs, known as H embrittlement. Despite ongoing research, the mechanisms behind H embrittlement remain a topic of debate [9–11]. At present, two different mechanisms have been widely accepted. One is the H-enhanced de-cohesion (HEDE) [12], and the other one is the H-enhanced local plasticity (HELP) [13,14]. The former states that H has a tendency to concentrate around the crack tip, lowering the fracture energy and ultimately resulting in a failure mechanism similar to cleavage. The latter is ascribed to the enhanced

* Corresponding authors.
E-mail addresses: lyliang@buaa.edu.cn (L. Liang), jinshuo@buaa.edu.cn (S. Jin).

https://doi.org/10.1016/j.fusengdes.2023.114030
Received 7 July 2023; Received in revised form 11 October 2023; Accepted 16 October 2023
Available online 22 October 2023

mobility of the dislocation with the existence of H atoms in W. This enhanced mobility results from the shielding effect due to the individual dislocation interaction, and the decreased interaction energy between SIAs and dislocations [15].

Over the last several decades, researchers have extensively utilized atomistic simulations [9,16–22] to study the interaction behaviors between a crack and H atoms in materials. The aim of these investigations is to understand the underlying fracture mechanisms in the presence of H atoms. Hu et al. [16] conducted molecular dynamics (MD) simulations to study the process of crack propagation and found that it is involved with the nucleation and coalescence of voids. Terasaki et al. [17] investigated the interaction mechanism between a crack and H atoms in Fe and found that the presence of a substantial quantity of H can lead to rapid crack propagation without significant plastic deformation. This phenomenon can be attributed to the lattice decohesion with the presence of H atoms. They also [18] focused on the interaction between H atoms and a crack in Fe and discovered that H atoms located close to the crack tip induce lattice distortion, structure decohesion, and a decrease in strength. Wang et al. [19] conducted an investigation on the fracture behaviors of α-Fe, focusing on the dissolution and absorption of H atoms. Results showed that the local distribution of H is a crucial factor in determining whether it promotes crack propagation or inhibits crack propagation when H atoms aggregate near the crack tip. Song et al. [9] examined how the mechanical properties of pre-cracked Fe are controlled by the concentration and distribution of H with a pre-existing crack and concluded that Fe shows good ductility when H atoms aggregate close to the crack tip. Furthermore, Xing et al. [20] examined the crack propagation in Fe by using MD simulations and discovered that Fe shows good brittleness when H atoms form an H-rich region around the crack tip. The influence of H atoms on dislocations near a crack tip was also studied to understand the interaction mechanism between H atoms and a crack. Taketomi et al. [21] explored the impact of H atoms on the dislocation emission from a crack tip in Fe through molecular statics analysis. They concluded that the presence of H atoms close to the crack tip enhances the emission of dislocations. They also [22] investigated the impact of H atoms on the motion of the {112}<111> dislocation and concluded that a decrease in dislocation mobility with a H concentration of 1.24/nm (the number of H atoms per unit length of the dislocation line). Despite both W and Fe being BCC metals, they exhibit distinct mechanical properties. For example, the single crystal W is highly brittle and only exhibits ductility until the temperature reaches 450 K [6] whereas Fe remains ductile until the temperature reaches 141 K [23]. Yu et al. [24] focused on the effect of the H concentration on the propagation of a crack in single crystal W. They concluded that the ductility of W can either be enhanced or diminished, depending on the H concentration. They also found that W exhibits cleavages along the {110} plane, which contradicts the experimental observations indicating a preference for {100} cleavage [25,26]. Despite many studies that have been conducted to explore the propagation behaviors of a crack with the presence of H atoms in W, the current understanding in this area remains insufficient to fully comprehend their interaction mechanisms.

In this study, we conduct an investigation on the interaction mechanism between a crack and H atoms in W using MD simulations at various temperatures and uniaxial strain loading conditions. Our study involves the calculation of surface energies of different planes in W as well as the analysis of the tensile behaviors in different tensile directions. Additionally, we simulate the crack propagation along three different tensile directions. The effects of temperature, strain rate, and H atoms on crack propagation are analyzed. The current results provide a comprehensive understanding of the effect of H atoms on the crack propagation in W, which may help to understand the interaction mechanism of H atoms and a crack in W.

We organize the structure of the paper as follows: Section 2 presents the employed simulation methods and simulation details. Section 3 gives the MD simulation results and discussion. The main conclusions are summarized in Section 4.

2. Simulation methods and details

We first construct a bulk single crystal W with periodic boundary conditions applied for all directions to study its deformation properties. The simulation domain has a size of $53 \times 43 \times 31\ a_0^3$, where a_0 represents the lattice constant of W having a value of 3.14 Å. NPT ensemble is used to relax the whole system with a time step of 2.0 fs for 20.0 ps. Then, we construct a rectangular simulation domain of W, incorporating a pre-existing crack. The dimensions of the simulation domain are set as $40 \times 8 \times 80\ a_0^3$. To construct a crack in the simulation domain, we remove a triangular region of W atoms. The crack length and width are set as 1.0 nm and 0.6 nm, respectively. Four-layer atoms are fixed by freezing them on constant lattice sites in the top and bottom layers of the simulation domain. The schematic diagram of the simulation domain is depicted in Fig. 1, where the red color denotes the frozen atom layers near the boundary, and the blue color represents the mobile part in the middle. Several previous work [27–31] studied the interaction between H and W under applied stresses using Wang's EAM potential [32] and produced reasonable results. Therefore, we employ Wang's EAM potential in this work. We use a canonical ensemble (NVT) for the mobile part (blue part), where the temperature is maintained as a constant by using the Nose-Hoover thermostat approach method. We relax the system using the conjugate gradient method. Non-periodic and shrink-wrapped boundary conditions are applied at all domain boundaries.

We analyze the crack propagation under a certain tensile load along three different directions in W. To ensure consistent application of the tensile load along the z-direction, we adjust the coordinate of the simulation domain in three different case A, B, and C. In the case of A, the *x, y*, and *z*-axis is chosen to be the [100], [010], and [001] direction, respectively. For the case of B, the *x, y*, and *z*-axis is chosen to be $[\bar{1}10]$, [001], and [110] direction, respectively. In the case of C, the *x, y*, and *z*-axis corresponds to the $[\bar{1}\bar{1}2]$, $[1\bar{1}0]$, and [111] direction, respectively. To account for the effect of the strain rate on the crack propagation, we consider three different constant strain rates of $1 \times 10^7\ s^{-1}$, $2 \times 10^8\ s^{-1}$, and $1 \times 10^9\ s^{-1}$.

To study the effect of H atoms on the crack propagation in W, H atoms are introduced in the semi-circle part of the domain randomly, as depicted in Fig. 1. The configuration of H atoms is not specified. The semi-circle part has a radius of 6.825 nm. The H concentration is quantified as $\frac{N_H}{N_{HT}} \times 100$ %, where N_H and N_{HT} represents the number of H atoms and the total number of atoms in the simulation domain, respectively. According to a previous experimental study [33], the concentration of H can be up to 10 % at 230 K. In this work, 500 H atoms are introduced to W, which corresponds to a H concentration of 3.9 %.

Based on the Virial theorem, the stress of the system can be calculated by [34],

$$\sigma^{mn} = \frac{1}{\Omega}\left\{ -\sum_i k_i v_i^m v_i^n + \frac{1}{2}\sum_i \sum_{j \neq i} \left(-\frac{1}{r_{ij}} \frac{\partial U}{\partial r_{ij}} \right) r_{ij}^m r_{ij}^n \right\} \quad (1)$$

where m and n denote Cartesian components, and i and j represent the atom i and j. Ω, k_i, and v_i is the volume of the simulation domain, mass, and velocity of atom i, respectively. r_{ij} is the magnitude of the displacement from atom i to j, and r_{ij}^m is the mth component of r_{ij}. All MD simulations presented in this work are performed using the large-scale atomic/molecular massively parallel simulator (LAMMPS) [35]. The Common Neighbor Analysis (CNA) technique in the OVITO software [36] is used to visualize the atomic structures. Dislocations and their Burgers vectors are identified using the dislocation extraction algorithm (DXA) in OVITO.

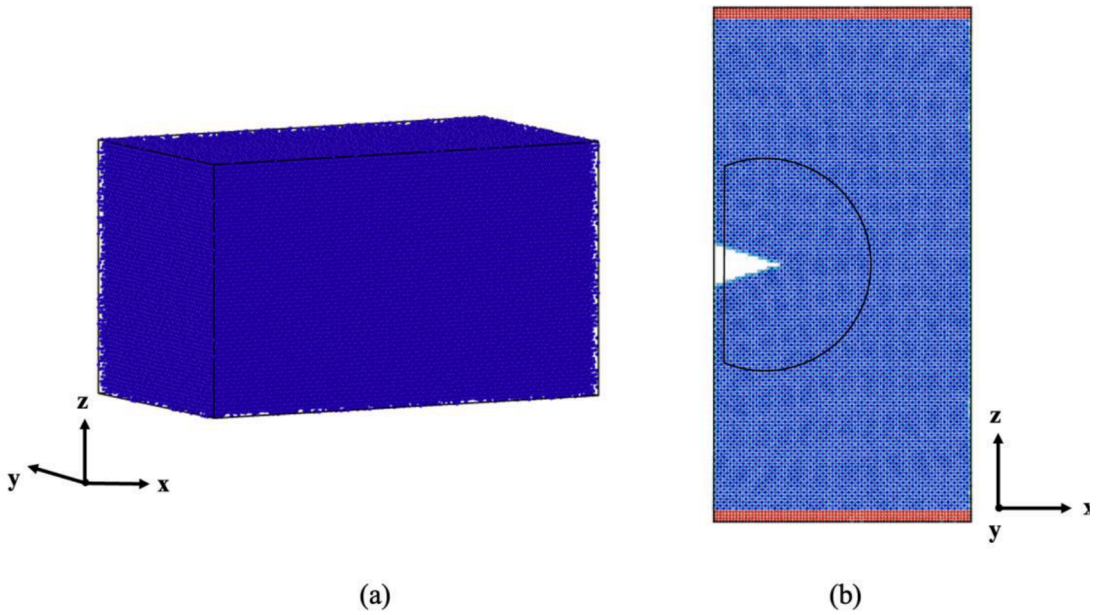

Fig. 1. The schematic diagram of (a) single crystal W, (b) simulation domain with a pre-existing crack.

3. Results and discussions

We first present the surface energies and tensile behaviors of the single crystal W. Then, we investigate the effects of the direction and the tensile strain rate and temperature on the tensile behaviors of the pre-cracked W. Finally, we study the effect of H atoms on crack

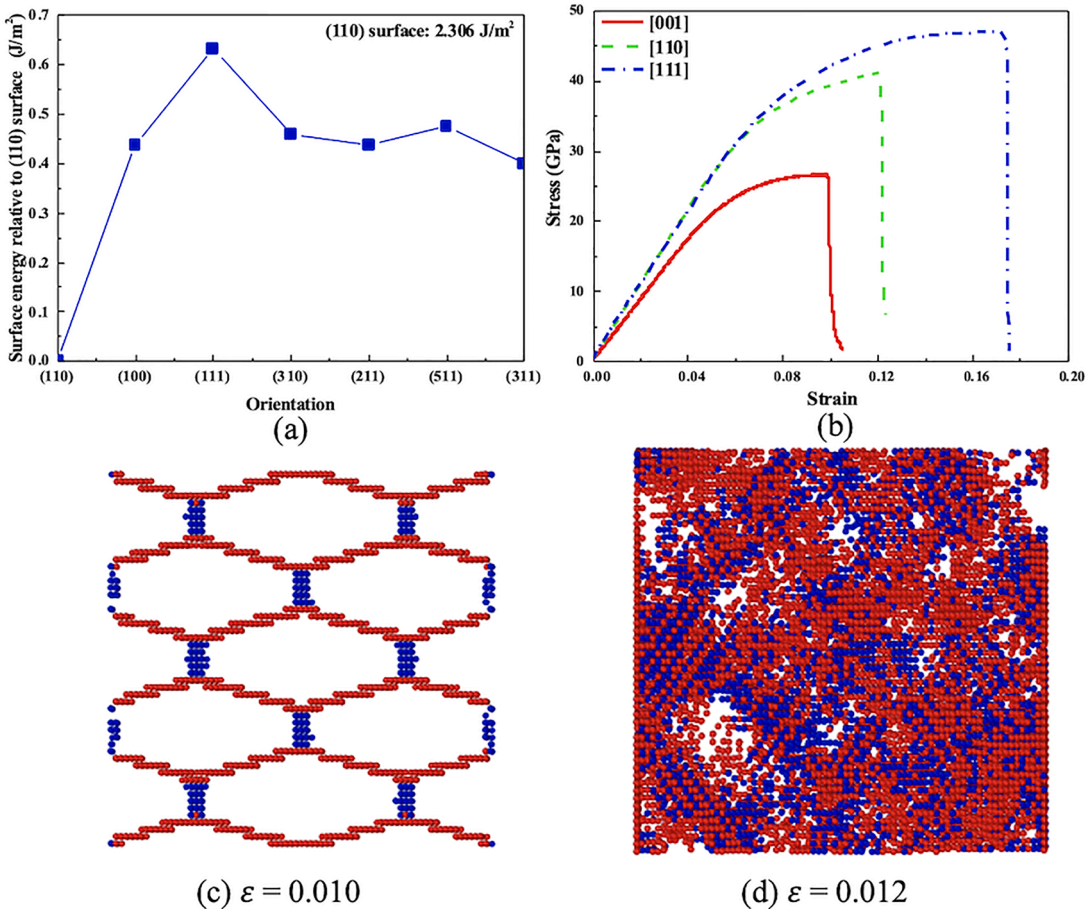

Fig. 2. (a) Surface energy relative to that of the (110) plane (b) Stress-strain curves with the applied tensile strain along three different directions in pure W. Atomic configuration of bulk W when tensile along [110] direction at the strain of (c) 0.10, (d) 0.12, where vacancies are painted in red while the interstitials were painted in blue. (For interpretation of the references to colour in this figure legend, the reader is referred to the web version of this article.).

propagation. The analysis and discussion about the crack propagation with or without H in W are also presented.

3.1. Fundamental properties of W

We first calculate the surface energies of seven different planes for W, as shown in Fig. 2(a). The surface energy of the (001), (110), and (111) planes is determined to be 2.743 J/m2, 2.305 J/m^2, and 2.935 J/m^2, respectively, which are consistent with previous MD simulation results [37]. Among these three planes, the (110) surface has the lowest surface energy, while the (111) surface has the highest surface energy. This observation aligns with the Density Functional Theory calculation result that the (110) surface possesses a lower surface energy compared to the (111) surface [38]. According to Griffith's theory, fracture energy is related to the surface energy of two newly formed fracture surfaces [39]. The lower the surface energy, the easier it is to cleavage fracture. In other words, the cleavage fracture is more likely to occur on the (110) plane because it has the lowest surface energy compared to the other two planes [40]. However, experimental results indicated a tendency for cleavage fractures to occur on the (001) plane. [25,26]. This contradiction suggests that the surface energy is not sufficient to explain the cleavage behavior in BCC metals.

To understand the cause of this contradiction, we conducted a uniaxial tension loading on pre-cracked W samples in different directions with a stain rate of 2×10^8 s^{-1}. The simulation temperature is set as 300 K. The tensile directions are chosen to be [001], [110], and [111] directions. The calculated stress-strain curves for these three different applied strain directions are presented in Fig. 2**(b)**. In fact, all three stress-strain curves exhibit a similar trend. With an initial linear increase in stress as the strain increases, followed by nonlinear stress increments, ultimately reaching a peak stress value referred to as the ultimate tensile stress (UTS). Fig. 2**(c)** shows the existence of vacancies at the strain rate of 0.10. With increasing the strain, vacancies migrate and aggregate to form voids at a strain rate of 0.12. The stress decreases dramatically with the increase of the strain, vacancies aggregate to form voids in W, as showb in Fig. 2(d). Based on the obtained strain-stress curves, UTS is determined to be 26.56 GPa, 41.06 GPa, and 46.84 GPa along the [001], [110], and [111] tensile direction, respectively. The UTS exhibits a maximum value when the applied stress is along the [111] direction and a minimum value along the [001] direction. This observed correlation between UTS and the direction of applied tensile stress in W is consistent with previous MD simulations [41]. Thus, the selection of the tensile direction significantly influences the mechanical properties of W.

3.2. Tensile behaviors of the pre-cracked W

3.2.1. Effect of the applied strain direction on the tensile behavior

We investigate the direction dependence of tensile behaviors of the pre-cracked W along the [001], [110], and [111] directions, respectively.\. The simulation is conducted at a temperature of 300 K and an applied strain rate of 2×108 s^{-1}. Fig. 3 depicts the stress-strain curves along three different directions in the pre-cracked W. The stress-strain curves exhibit a significant difference among three cases with different applied strain rates. The elastic modulus, determined from the slopes of the stress-strain curves within a limited strain range, is highest along the [110] direction and lowest along the [111] direction. This indicates that the [110] tensile direction has the greatest resistance to elastic deformation compared to the other two directions.

Fig. 4 gives the snapshots of the atomic structure of the pre-cracked W during the crack propagation along the [001], [110], and [111] directions at three different chosen strain rates. The BCC structured W changes into a disordered structure under applied tensile strains and is colored white, as shown in Fig. 4**.** When the applied tensile load is along the [001] direction, the 1/2<111> dislocation with different directions can be observed in Fig. 4 **(a,b)**. At the strain of 0.1, the crack propagates along the [010] direction that is the *y*-axis, as shown in Fig. 4**(c)**. This is due to the release of 1/2<111> dislocations in different directions. And as a BCC transition metal, experiments showed that the cleavage usually occurs on the (100) plane in Fe, Mo, and Nb [42,43]. When the applied tensile strain is along the [110] direction, a BCC structure around the crack tip changes into a disordered structure. Fig. 4**(d)** shows dislocations can be observed in front of the crack tip at a tensile strain of 0.031. Then the slip of dislocations induces small-sized voids to appear in the slip path of the dislocation, which is shown in Fig. 4**(e)** when the strain reaches 0.063. With increasing strain, these voids grow and coalesce and finally lead to a substantial void, which creates new surfaces and can contact the crack tip, as shown in Fig. 4**(f)**. This helps the propagation of the crack. During this process, the interaction between voids and dislocations may change the slip direction of the dislocation. In the case of applied tensile strain along the [111] direction, no dislocation emissions are observed and the crack propagates very rapidly. This is reasonable because the [111] direction presents as one of the slip directions in the BCC crystal, as shown in Fig. 4 **(g, i)**.

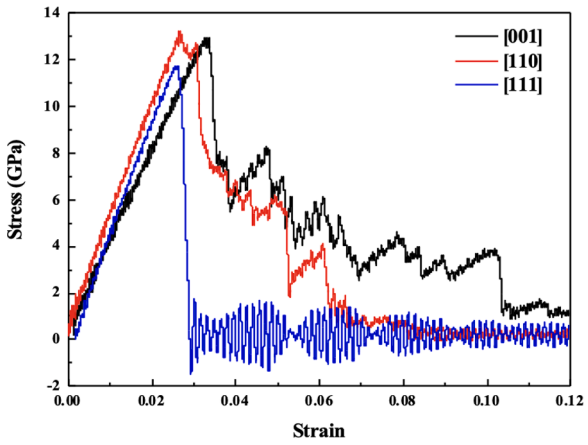

Fig. 3. Stress-strain curves with the applied tensile strain along three different directions in the pre-cracked W.

From the presented atomic structures of the pre-crack W in Fig. 4 **(a-c)** and **(g-i)**, it is difficult to observe the plastic deformation along [001] and [111] directions. To gain deep insights into the plastic deformation and the slip of the dislocation close to the crack tip, the (110) direction is thus selected as the tensile direction to investigate the effects of the temperature, strain rate, and H atoms on the behaviors of crack propagation in W.

3.2.2. Effect of the temperature on the tensile behavior

The stress-strain curves of the pre-cracked W under six different temperatures are simulated, employing a tensile strain rate of 2×10^8 s^{-1} applied along the [110] direction. Fig. 5**(a)** presents the stress-strain curves at six chosen simulation temperatures. Throughout the elastic deformation stage, the stress exhibits a linear increase with increasing strain for all six simulation cases. Subsequently, as the strain increases, corresponding decreases in stress are observed. The relationship between UTS and temperature is given in Fig. 5**(b)**. UTS decreases as the temperature increases. A similar relationship between UTS and temperature is observed in Fe [44,45]. At high temperatures, enough energy can be provided for dislocation activation, promoting dislocation nucleation. Also, the dislocation can overcome the resistance of dislocation motion with the assistance of thermal vibration at high temperatures [46].

To comprehend the effect of temperature on the crack propagation in W, Fig. 6 illustrates the atomic structure evolution during the tensile process at three different temperatures, 300 K, 800 K, and 1200 K are selected. At 300 K, the crack opening displacement increases with increasing strain during the initial stage of crack propagation. This is attributed to both the lattice distortion and the accumulation of stress

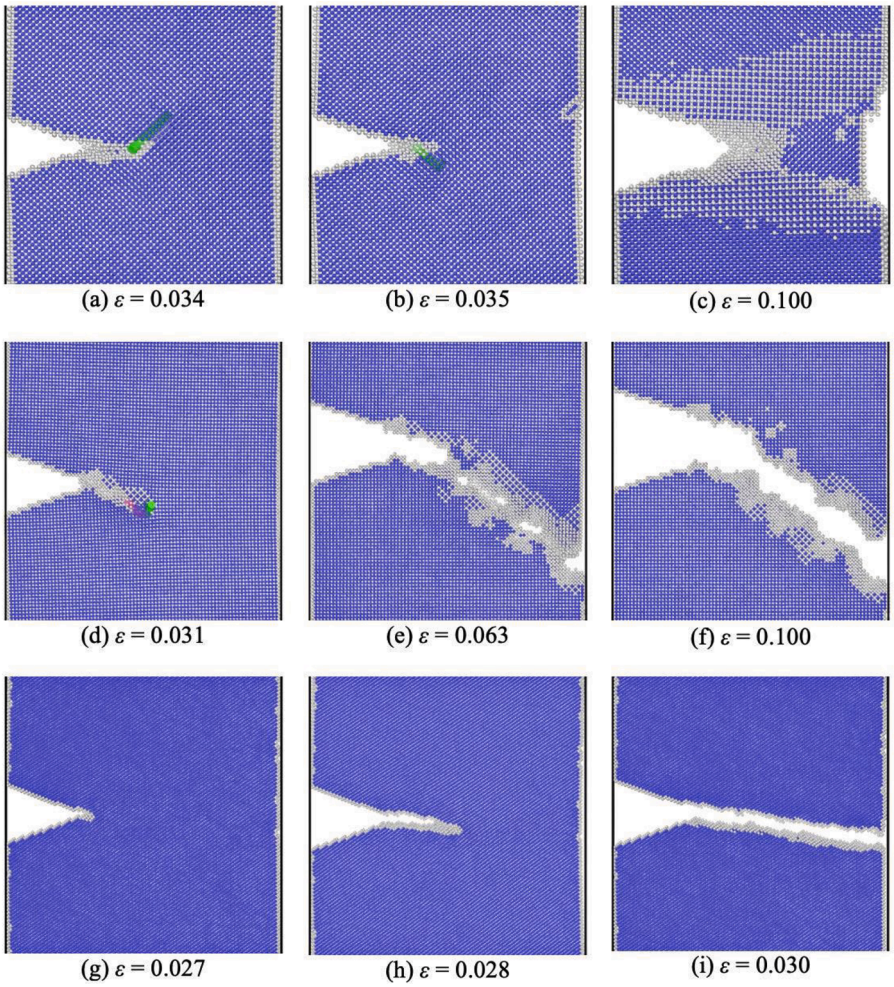

Fig. 4. Atomic configuration of the pre-cracked W (a-c) under the applied [001] tensile direction, (d-f) under the applied [110] tensile direction, and (g-i) under the applied [111] tensile direction at different strains.

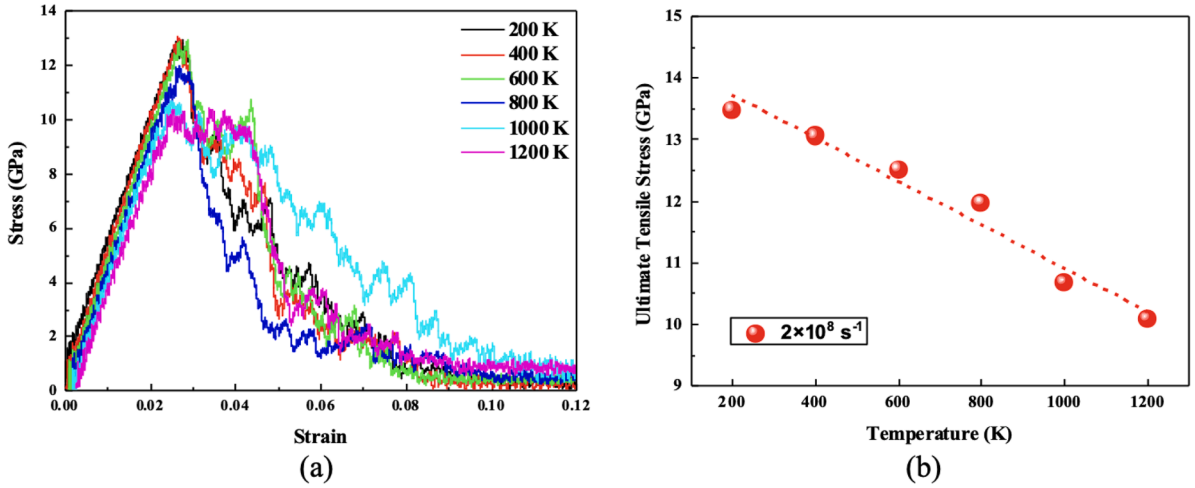

Fig. 5. (a) Stress-strain curves at six different temperatures. (b) UTSs as a function of the temperature in the pre-cracked W. The dotted line is the linear fitting curve of UTS as a function of temperature.

concentration at the crack tip increasing with the increasing strain. When the strain reaches 0.035, the voids form and the crack propagates, as shown in Fig. 6 **(b,c).** The evolution of the atomic structure during the crack propagation at 800 K exhibits similarities to that at 300 K. When the simulation temperature is set at 1200 K, the crack tip becomes blunted as shown in Fig. 6**(h).** This phenomenon occurs because the release of the stress concentration around the crack tip. W atoms can easily move back to equilibrium positions due to their large kinetic

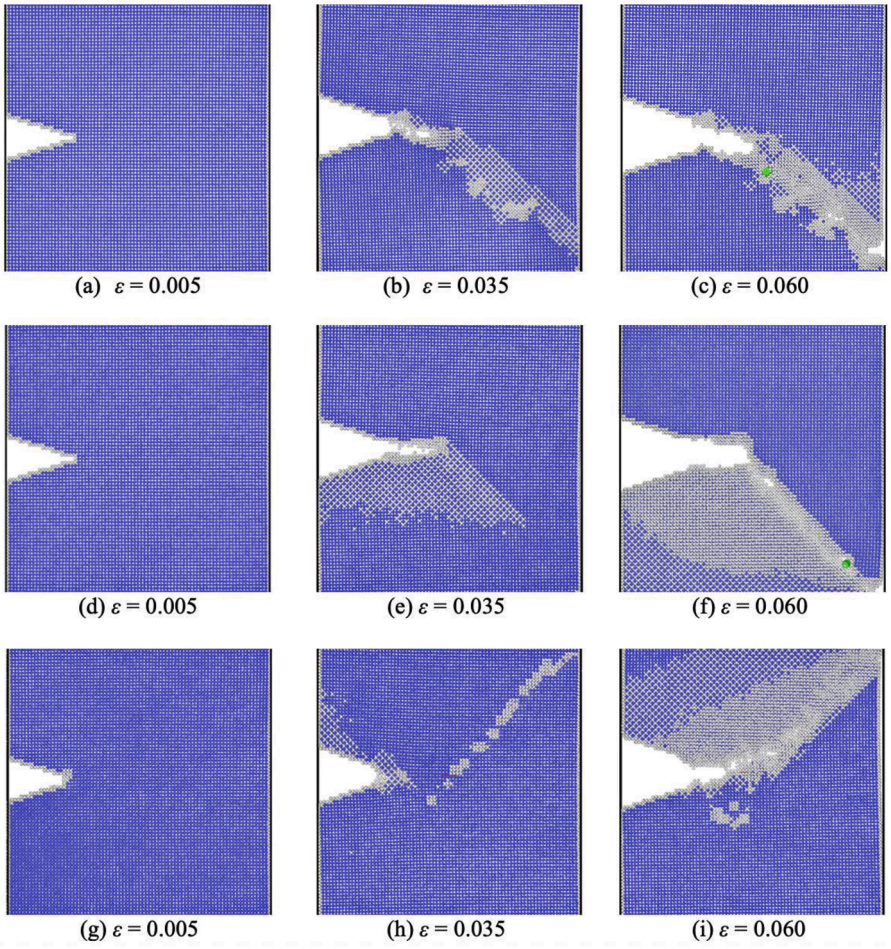

Fig. 6. Atomic configuration of the pre-cracked W under the strain rate of 2×10^8 s^{-1} at three temperatures: (a-c) 300 K; (d-f) 800 K; (g-h) 1200 K.

energies at high temperatures. And when the applied strain reaches 0.035 as exhibited in Fig. 6**(h)**, the crack tip is blunted compared to it in Fig. 6**(g)**. A comparison of the crack propagation length along the *y*-axis direction at a strain of 0.06 in Fig. 6 reveals that crack propagation is slower at higher temperatures. In essence, as the temperature increases, the crack propagation rate decreases.

3.2.3. *Effect of the strain rate on the crack propagation*

We study how the strain rate influences crack propagation in the pre-cracked W. The relationship between the UTS and temperature is plotted in Fig. 7, considering three different selected strain rates of 1×10^7 s^{-1}, 2×10^8 s^{-1}, and 1×10^9 s^{-1}. We employ a linear line to fit the UTS as a function of temperatures. The values of UTS at different strain rates generally decrease with increasing temperature, a trend is consistent with previous simulation findings in both W [47] and Fe [48]. This is caused by the assistance of the thermal vibration on dislocation motion at high temperatures. Generally, the values of UTS increase with the increasing applied strain rate, except for the case under strain rates of 1×10^7 s^{-11} and 2×10^8 s^{-1} when the temperature is 400 K and 1200 K. Based on the Orowan's equation [49], the velocity and density of the dislocation are proportional to the strain rate. At high strain rates, UTS increases to accommodate the increase of the dislocation velocity. Therefore, it is reasonable that the UTS is large at high strain rates.

To get comprehensive insights into the influence of the strain rate on the crack propagation of W, we provide the atomic structure evolution throughout the crack propagation. The plastic deformation can be observed under high-temperature conditions. We set the simulation temperature at 1200 K to observe the plastic deformation near the crack

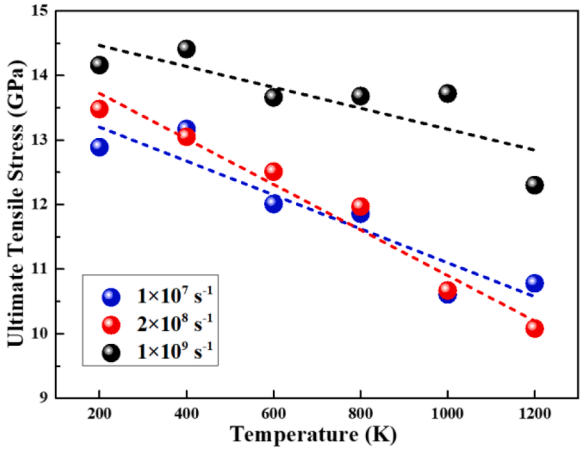

Fig. 7. UTS as a function of the temperature under three different applied strain rates in the pre-cracked W. The dots are the calculated values of UTS. UTSs at the strain of 1×10^7 s^{-1}, 2×10^8 s^{-1}, and 1×10^9 s^{-1} are colored blue, red, and black, respectively. The lines are linear fitting curves of UTSs at three different strain rates. (For interpretation of the references to colour in this figure legend, the reader is referred to the web version of this article.).

tip. Fig. 8 illustrates the sequential snapshots of the atomic configuration throughout the crack propagation in pre-cracked W under strain rates of 1×10^7 s^{-1} and 1×10^9 s^{-1}. Fig. 6 **(g-i)** exhibits the observed atomic structures at the strain rate of 2×10^8 s^{-1}. For the strain rate of 1×10^7

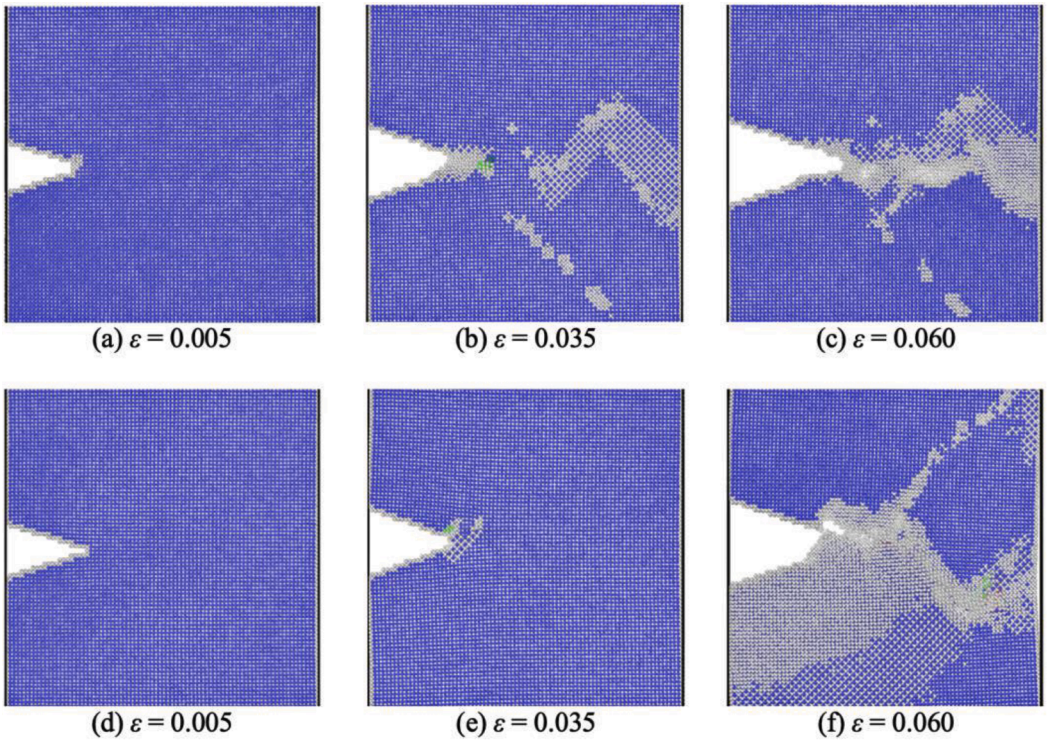

Fig. 8. Atomic configuration of the pre-cracked W at 1200 K under the strain rate of (a-c) $1 \times 10^7\ s^{-1}$ and (d-f) $1 \times 10^9\ s^{-1}$ at different tensile strains.

s^{-1}, Fig. 8**(a)** shows a phase transition at the crack tip. At a strain of 0.035**,** a 1/2<111> dislocation can be observed ahead of the crack tip, with slip traces of dislocations visible as shown in Fig. 8**(b)**. Fig. 8**(c)** exhibits a relatively shorter crack propagation length near the crack tip when the strain reaches 0.060, in comparison to Fig. 8**(b)**. Under the strain rate of $1 \times 10^9\ s^{-1}$, it can be clearly observed that the crack tip opening displacement increases with the increasing strain. As the strain reaches 0.035, the crack tip opening displacement exhibits a notably greater magnitude compared to the strain of 0.005. And as the strain reaches 0.060, voids are found to form ahead of the crack tip as presented in Fig. 8**(f)**. The crack length is smaller than that of $2 \times 10^8\ s^{-1}$, as shown in Fig. 6**(h)**.

At the strain rate of $1 \times 10^9\ s^{-1}$, a significant quantity of dislocations is emitted from the crack tip, releasing the stress near the crack tip, which induces the blunting of the crack tip and impedes the crack propagation. At high strain rates, atoms do not have sufficient time to rearrange or reorganize themselves to the lattice sites. This leads to an increase in the chance of the generation of dislocations. Furthermore, high strain rates lead to the emission of dislocation in order to release the stress at the crack tip. These findings closely resemble those reported in a prior investigation conducted on Ni [50]. Generally, as the strain rate increases, the crack propagation length decreases owing to the emission of dislocations around the crack tip.

3.3. Hydrogen effect on crack propagation

3.3.1. Surface energy

Due to its involvement as a which serve as a raw material in the nuclear fusion reaction, H atoms significantly impact the mechanical properties of pre-crack W. H atoms are randomly introduced around the crack tip in W. Fig. 9 **(a,b)** show the lattice structure and atomic structure of W with 500 H atoms are introduced at 300 K at the strain of 0.001, respectively. H and W atoms are colored red and blue in Fig. 9**(b)**, respectively. Comparing the distribution of atoms in Fig. 9 **(a,b)**, the atoms with a BCC structure occupied by H atoms transform into a disordered structure. Thus, H atoms in W can cause a lattice distortion

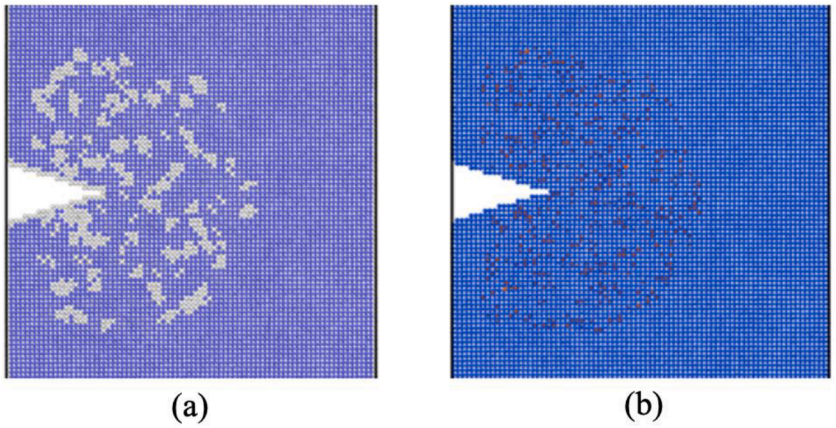

Fig. 9. The (a) lattice structure and (b) atomic structure of the pre-cracked W at a strain of 0.001.

[51].

Subsequently, we evaluate the influence of H concentration on the surface energy of the (110) plane in W. Initially, the simulation domain contains a random distribution of H atoms. The variation of the surface energy with respect to the H concentration in W is shown in Fig. 10. With increasing H concentration, the surface energy decreases linearly. A similar relationship between surface energy and H concentration was observed in a previous MD simulation study conducted on Fe [52]. Therefore, the introduction of H atoms in W can decrease its surface energy.

3.3.2. Temperature effect

Subsequently, we examine the crack propagation in pre-cracked W containing H atoms at different temperatures. Specifically, we investigate the case where 500 H atoms are introduced to W and an applied strain rate is $2 \times 10^8\ s^{-1}$. The evolutions of the atomic structures at 300 K, 800 K, and 1200 K are shown in Fig. 11. At 300 K, Fig. 11**(a)** shows the atomic structure under a strain of 0.005. A void is formed ahead of the crack tip when the strain increases to 0.4, as seen in Fig. 11**(b)**. At a strain of 0.060, the crack propagates as a result of the interaction between the growing void and the crack tip, as illustrated in Fig. 11**(c)**. Comparatively, in the presence of H atoms at 300 K, the crack propagation is hindered, as seen in Fig. 6 **(a-c)**. Similarly, in the presence of H atoms, the crack grows relatively slower compared to the case without H atoms [9]. The presence of H atoms in front of the crack can impede its propagation, resulting in slow crack propagation around the crack tip. This aligns with the observation that voids are generated in front of the crack tip when H atoms are introduced to W, as evidenced by the comparison between Figs. 6**(f)** and 11**(b)**. Previous studies consistently shows that introducing H atoms facilitates the initiation, expansion, and merging of voids in steel [53,54]. When the temperature increases to 800 K, fewer H atoms remain in W compared to the case at 300 K, as shown in Fig. 11**(d)**. The difference can be ascribed to the enhanced mobility of H atoms at high temperatures, causing more H atoms to diffuse to the W surface and fewer H atoms remaining in the bulk of W. Additionally, as strain increases, some H atoms tend to accumulate within the slip trace of the dislocation located ahead of the crack tip, as shown in Fig. 11**(e)**. A previous MD simulation study suggested that H atoms adhere to the 1/2<111> edge dislocation core and move along with it when the temperature in W is below 1300 K [55]. Under the applied tensile load, H atoms can accumulate around the crack tip and decrease the surface energy of the plane around the crack tip. The crack can easily propagate along the plane with a high H concentration. This agrees with a previous study that the crack prefers to propagate along the surface with a high H concentration in Fe [56]. With increasing strain, numerous voids are formed within the slip trace of the dislocation, as shown in Fig. 11**(f)**. In comparison to the case without H, as shown in Fig. 6 **(d-f)**, the presence of H inhibits crack propagation. At 1200 K, Fig. 11**(g)** shows that fewer H atoms are present in W compared to that found in Fig. 11**(a)** at 300 K and in Fig. 11**(d)** at 800 K. As the strain continues to increases, part of H atoms migrate to the slip trace of dislocation, leading to a minor extension in the crack length, as shown in Fig. 11**(h).** When the strain reaches 0.060, the fracture of W is observed. Generally, at high temperatures, the plastic deformation of metals is enhanced, making them more ductile. Furthermore, the crack propagation rate can be reduced by H atoms in front of the crack tip. Therefore, it is anticipated that the crack is blunted at high temperatures. However, W fractures at 1200 K. This occurs due to the presence of the dislocation slip and H atoms, which enhances the formation of voids. Both the coalescence of formed voids and the decreased surface energy induced by H atoms along the slip trace ultimately lead to rapid crack propagation and the final fracture of W, as shown in Fig. 11**(f)**. Therefore, H atoms can impede the propagation of the crack at low temperatures. These atoms migrate to dislocation slip traces, facilitating the crack propagation and further fracture of W at high temperatures.

3.3.3. Strain rate effect

We then study the crack propagation with H atoms in the pre-cracked W by varying strain rates. Three different strain rates of $1 \times 10^7\ s^{-1}$, $2 \times 10^8\ s^{-1}$, and $1 \times 10^9\ s^{-1}$ are selected. Fig. 12 shows the atomic structures of the model under these three strain rates with 500 H atoms at 1200 K. For the strain rate of $1 \times 10^7\ s^{-1}$, Fig. 12**(a)** shows few H atoms are present in W, with some of them aggregating around the crack tip. This occurrence can be attributed that H atoms have sufficient time to migrate to the surface of W at low strain rates. With the increasing strain, fewer H atoms exist in W, and the remaining H atoms tend to concentrate near the crack tip, as shown in Fig. 12**(b)**. At a strain of 0.060, the crack propagates along the plane with a high concentration of H atoms, as shown in Fig. 12**(c)**. Compared to the W without H at the strain rate of $1 \times 10^7\ s^{-1}$ in Fig. 8**(c)**, the crack propagation is enhanced

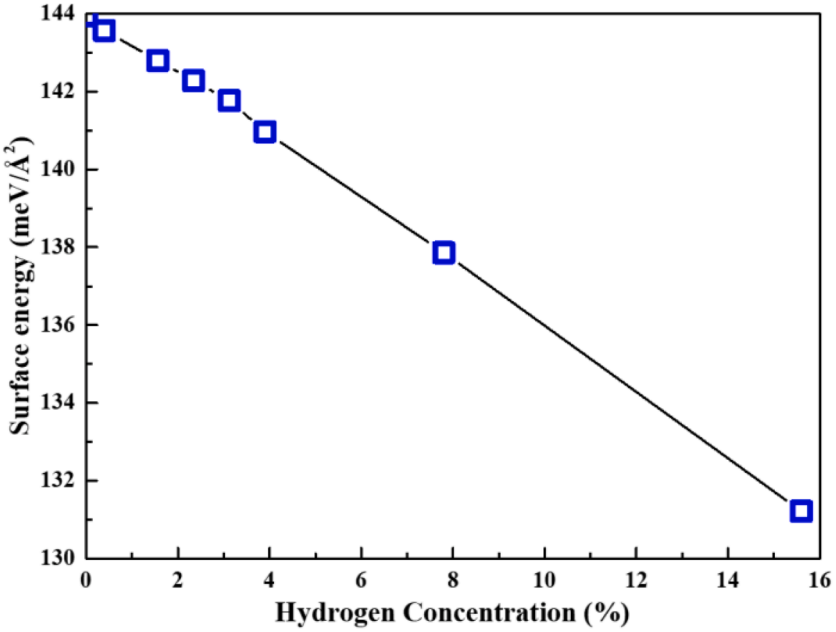

Fig. 10. The relationship of H concentration and the surface energy of the (110) plane.

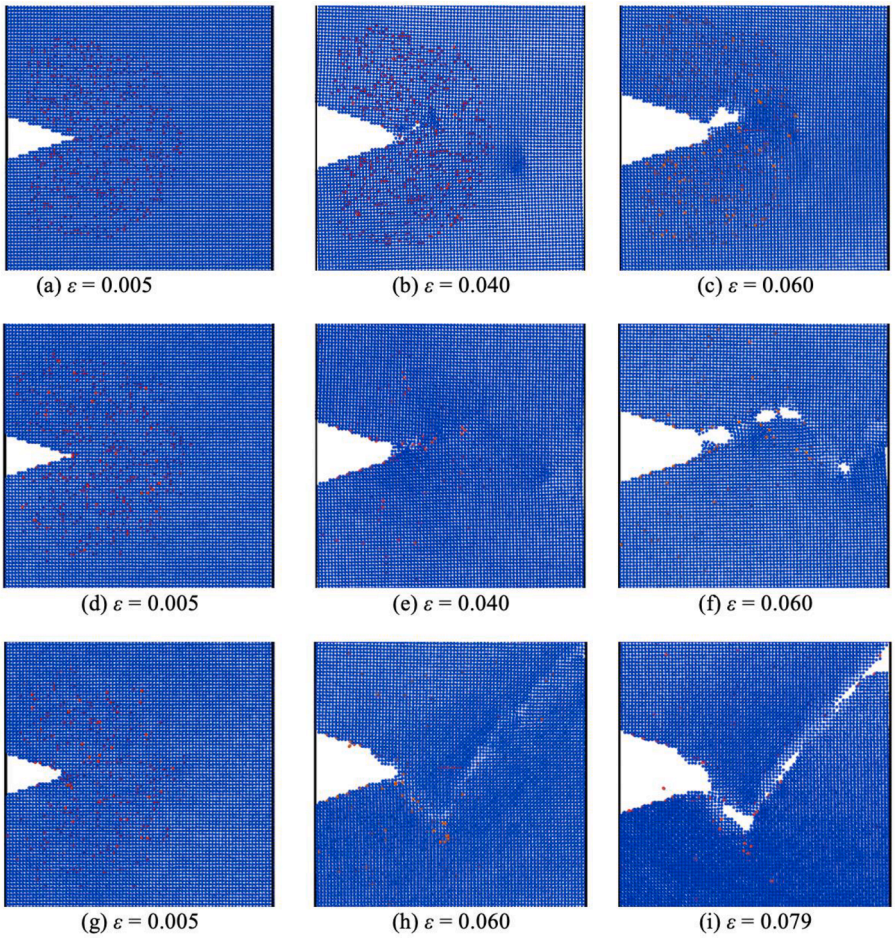

Fig. 11. Atomic configuration with 500 H atoms of the pre-cracked W at the temperature of (a-c) 300 K, (d-f) 800 K, and (g-i) 1200 K under different tensile strains.

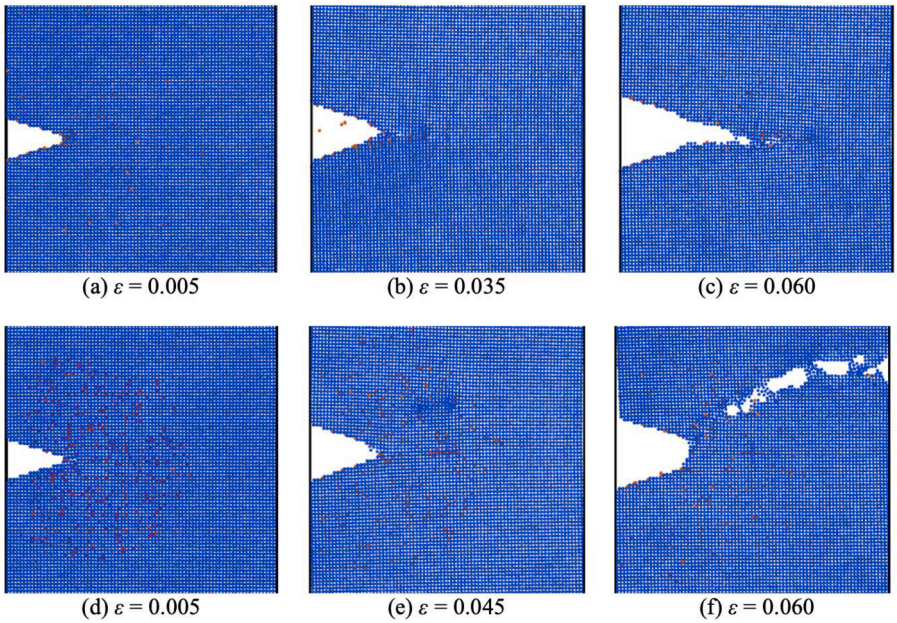

Fig. 12. Atomic configuration of the pre-cracked W in the presence of 500 H atoms under the strain rate of (a-c) $1 \times 10^{7}\ s^{-1}$and (d-f) $1 \times 10^{9}\ s^{-1}$ at different tensile strains at 1200 K.

in the presence of H atoms. Previous experiments [57] showed that Fe-C becomes brittle and the crack propagation is enhanced when low strain rates are applied, which can be related to the diffusion properties of H atoms at low strain rates. According to a previous study [58], the presence of H atoms can accelerate the propagation of W cracks when the cyclic loading rate slows down. Also, an experimental result in steel [59] showed that with a decrease in strain rate, the plasticity of steel significantly decreases. Fig. 11 **(d-f)** show the snapshots of atomic structures during the crack propagation at the strain rate of $2 \times 10^8\,s^{-1}$. The number of remaining H atoms in W is higher than that observed at a strain rate of $1 \times 10^7\,s^{-1}$, as shown in Fig. 11**(d)**. For the strain rate of $1 \times 10^9\,s^{-1}$, Fig. 12**(d)** shows a significant amount of H atoms still present in W at a strain of 0.005. At a strain of 0.045, the dislocation slips result in the blunting of crack tip, while voids are formed in the slip trace away from the crack tip and then grow, as shown in Fig. 12 **(d-f).** In contrast to W without H atoms at a strain rate of $1 \times 10^9\,s^{-1}$, as shown in Fig. 8**(d)**, voids are formed near the crack tip instead of the slip traces away from the crack tip, as shown in Fig. 12**(f)**. These voids situated away from the crack tip tend to enlarge and merge, instead of interacting directly with the crack tip. This phenomenon causes crack propagation to slow down at high strain rates. In general, the crack propagation is impeded by the increase in the strain rate. The results of crack propagation at different strain rates and temperatures indicate that the diffusion velocity of H atoms may be a key factor influencing material properties.

In MD simulation, the loading rate is usually many orders of magnitude higher than that of actual experiments, which may introduce a disparity when comparing the MD simulation results with experimental data. Due to the mismatch in time scales, MD simulation results capture behaviors on an atomic-level time scale that may not reflect the experimental process at the microscopic scale. Additionally, a high loading rate can introduce dynamic effects such as shockwaves or rapid stress waves, that are rarely observed in slow-loading experiments. Although MD simulations can provide valuable insights into the atomic-scale behaviors of materials and help to understand the underlying mechanisms, their results should be considered as complementary to experimental data. Therefore, the current study can provide an atomic interaction mechanism between the H atoms and W, which may help to understand the fracture behaviors under loading conditions.

4. Conclusions

In this study, we employ the molecular dynamics method to study the effects of temperature, strain rate, and hydrogen (H) atoms on the propagation of a pre-existing crack in single crystal tungsten (W). Our simulation results demonstrate that the ultimate tensile stress (UTS) decreases with increasing temperature, which is consistent with previous simulation results. Increasing temperature can reduce the crack propagation rate. The plastic deformation can be observed from the atomic structure at high temperatures. When subjected to applied strain, we observe that the UTS tends to exhibit an increasing trend to accommodate the increased dislocation velocity as the strain rate increases. Dislocations are emitted from the crack tip at high strain rates, releasing the stress concentration and consequently leading to a slower rate of crack propagation. In the presence of H atoms in W, the propagation of the crack can be impeded at low temperatures, resulting in an increased ductility compared to the case without H atoms. However, as temperature increases, the slip of the dislocation promotes the formation of voids ahead of the crack tip, where the crack can easily propagate on the plane with high H concentrations. Consequently, both the coalescence of voids and the decreased surface energy caused by H atoms along the slip trace of dislocations accelerate crack propagation. Ultimately, this mechanism leads to the final fracture of W. Furthermore, as the applied strain increases, the crack tip becomes blunted, resulting in a reduced propagation rate. The phenomenon can be attributed to the formation of numerous voids along the dislocation slip trace, located away from the crack tip. These voids exhibit a propensity to grow and coalesce with each other instead of interacting with the crack tip at high strain rates. Also, the results of the crack propagation at different temperatures or strain rates in the presence of H atoms suggest that providing sufficient time for H atoms to migrate may be a key factor influencing the material properties of W. In conclusion, our simulation results provide a comprehensive insight into the influence of H atoms on the propagation of the crack in W, which may help to understand the H-induced embrittlement in W under irradiation conditions.

CRediT authorship contribution statement

Jun Shi: Methodology, Conceptualization, Formal analysis, Writing – original draft. **Bingchen Li:** Writing – review & editing. **Lei Li:** Data curation. **Yifan Liu:** Data curation. **Xinyue Fan:** Software. **Qing Peng:** Funding acquisition. **Linyun Liang:** Conceptualization, Writing – review & editing, Funding acquisition. **Shuo Jin:** Conceptualization, Investigation. **Guang-Hong Lu:** Supervision.

Declaration of Competing Interest

The authors declare that they have no known competing financial interests /personal relationships that coud have appeared to infuence the work reported in this paper.

Data availability

The data generated in this work can be made available upon reasonable request.

Acknowledgments

This research is supported by the National MCF Energy R&D Program of China with Grant No. 2018YFE0308103, and the National Natural Science Foundation of China with Grant Nos. 12075021, 12075023, and 12272378. LiYing Program of the Institute of Mechanics, Chinese Academy of Sciences with Grant No. E1Z1011001. Qing Peng appreciates the support from High-level Innovation Research Institute Program of Guangdong Province with Grant No. 2020B0909010003.

References

[1] J.M. Chen, X. Liu, P.H. Wang, P. Huang, J.B. Wang, L.Z. Cai, F.Y. Jin, X.B. Zhu, Q. Li, Y.Y. Chen, Z.X. Wei, M. Xu, X.R. Duan, Progress in developing ITER and DEMO first wall technologies at SWIP, Nucl. Fusion 60 (2019), 016005, https://doi.org/10.1088/1741-4326/ab483a.

[2] M. Kaufmann, R. Neu, Tungsten as first wall material in fusion devices, Fusion Eng. Des. 82 (2007) 521–527, https://doi.org/10.1016/j.fusengdes.2007.03.045.

[3] T.H. Kwon, S. Park, J.M. Ha, Y.-S. Youn, Study on sputtering yield of tungsten with different particle sizes: surface roughness dependence, Nucl. Eng. Technol. 53 (2021) 1939–1941, https://doi.org/10.1016/j.net.2020.12.024.

[4] Y.-Z. Jin, X. Liu, Y.-Y. Lian, J.-P. Song, Influence of recrystallization on tungsten divertor monoblock under high heat flux, Tungsten 4 (2022) 194–202, https://doi.org/10.1007/s42864-021-00126-1.

[5] G. Pintsuk, Tungsten as a plasma-facing material, Compr. Nucl. Mater. 4 (2012) 551–581, https://doi.org/10.1016/B978-0-08-056033-5.00118-X.

[6] R.G. Abernethy, J.S.K.-L. Gibson, A. Giannattasio, J.D. Murphy, O. Wouters, S. Bradnam, L.W. Packer, M.R. Gilbert, M. Klimenkov, M. Rieth, H.-C. Schneider, C. D. Hardie, S.G. Roberts, D.E.J. Armstrong, Effects of neutron irradiation on the brittle to ductile transition in single crystal tungsten, J. Nucl. Mater. 527 (2019), 151799, https://doi.org/10.1016/j.jnucmat.2019.151799.

[7] H. Chen, Q. Xu, J. Wang, P. Li, J. Yuan, B. Lyu, J. Wang, K. Tokunaga, G. Yao, L. Luo, Y. Wu, Effect of surface quality on hydrogen/helium irradiation behavior in tungsten, Nucl. Eng. Technol. 54 (2022) 1947–1953, https://doi.org/10.1016/j.net.2021.12.006.

[8] E. Lang, A. Kapat, T.W. Morgan, J.P. Allain, High flux helium irradiation of dispersion-strengthened tungsten alloys and effects of heavy metal impurity layer deposition, J. Nucl. Mater. 544 (2021), 152672, https://doi.org/10.1016/j.jnucmat.2020.152672.

[9] H.Y. Song, L. Zhang, M.X. Xiao, Molecular dynamics simulation of effect of hydrogen atoms on crack propagation behavior of α-Fe, Phys. Lett. A 380 (2016) 4049–4056, https://doi.org/10.1016/j.physleta.2016.10.019.

[10] I.M. Robertson, P. Sofronis, A. Nagao, M.L. Martin, S. Wang, D.W. Gross, K. E. Nygren, Hydrogen embrittlement understood, Metal. Mater. Trans. B 46 (2015) 1085–1103, https://doi.org/10.1007/s11663-015-0325-y.
[11] F. Dear, G. Skinner, Mechanisms of hydrogen embrittlement in steels: discussion, Philos. Trans. R. Soc. A Math. Phys. Eng. Sci. 375 (2017), 20170032, https://doi.org/10.1098/rsta.2017.0032.
[12] A. Troiano, The role of hydrogen and other interstitials in the mechanical behavior of metals, Edward de Mille Campbell memorial lecture, Trans. ASM 52 (1960) 54–80, https://doi.org/10.1007/s13632-016-0319-4.
[13] D.P. Abraham, C.J. Altstetter, Hydrogen-enhanced localization of plasticity in an austenitic stainless steel, Metal. Mater. Trans. A 26 (1995) 2859–2871, https://doi.org/10.1007/BF02669644.
[14] J. Song, W.A. Curtin, Mechanisms of hydrogen-enhanced localized plasticity: an atomistic study using α-Fe as a model system, Acta Mater. 68 (2014) 61–69, https://doi.org/10.1016/j.actamat.2014.01.008.
[15] M. Wagih, Y. Tang, T. Hatem, J.A. El-Awady, Discerning enhanced dislocation plasticity in hydrogen-charged α-iron nano-crystals, Mater. Res. Lett. 3 (2015) 184–189, https://doi.org/10.1080/21663831.2015.1052889.
[16] Z. Hu, S. Fukuyama, K. Yokogawa, S. Okamoto, Hydrogen embrittlement of a single crystal of iron on a nanometre scale at a crack tip by molecular dynamics, Model. Simul. Mater. Sci. Eng. 7 (1999) 541–551, https://doi.org/10.1088/0965-0393/7/4/305.
[17] N.T.F. Terasaki, T. Kawakami, A. Yoshikawa, Mechanism of crack propagation due to hydrogen embrittlement in iron single crystals stressed along [001]axis, Metal. Res. Technol. 95 (1998) 1519–1529, https://doi.org/10.1051/metal/199895121519.
[18] I.Y. Telitchev, O. Vinogradov, Numerical tensile tests of BCC iron crystal with various amounts of hydrogen near the crack tip, Comput. Mater. Sci. 36 (2006) 272–280, https://doi.org/10.1016/j.commatsci.2005.04.006.
[19] Z. Wang, X. Shi, X.-S. Yang, W. He, S.-Q. Shi, X. Ma, Atomistic simulation of the effect of the dissolution and adsorption of hydrogen atoms on the fracture of α-Fe single crystal under tensile load, Int. J. Hydrogen Energy 46 (2021) 1347–1361, https://doi.org/10.1016/j.ijhydene.2020.09.216.
[20] X. Xing, H. Zhang, G. Cui, J. Liu, Z. Li, Hydrogen inhibited phase transition near crack tip – an atomistic mechanism of hydrogen embrittlement, Int. J. Hydrogen Energy 44 (2019) 17146–17153, https://doi.org/10.1016/j.ijhydene.2019.04.205.
[21] S. Taketomi, R. Matsumoto, N. Miyazaki, Atomistic study of the effect of hydrogen on dislocation emission from a mode II crack tip in alpha iron, Int. J. Mech. Sci. 52 (2010) 334–338, https://doi.org/10.1016/j.ijmecsci.2009.09.042.
[22] S. Taketomi, R. Matsumoto, S. Hagihara, Molecular statics simulation of the effect of hydrogen concentration on {112} <111>edge dislocation mobility in alpha iron, ISIJ Int. 57 (2017) 2058–2064, https://doi.org/10.2355/isijinternational.ISIJINT-2017-172.
[23] M. Tanaka, E. Tarleton, S. Roberts, The brittle–ductile transition in single-crystal iron, Acta Mater. 56 (2008) 5123–5129, https://doi.org/10.1016/j.actamat.2008.06.025.
[24] X. Yu, F. Gou, B. Li, N. Zhang, Numerical study of the effect of hydrogen on the crack propagation behavior of single crystal tungsten, Fusion Eng. Des. 89 (2014) 1096–1100, https://doi.org/10.1016/j.fusengdes.2013.12.007.
[25] J. Riedle, P. Gumbsch, H.F. Fischmeister, V.G. Glebovsky, V.N. Semenov, Fracture studies of tungsten single crystals, Mater. Lett. 20 (1994) 311–317, https://doi.org/10.1016/0167-577X(94)90036-1.
[26] J. Riedle, P. Gumbsch, H.F. Fischmeister, Cleavage anisotropy in tungsten single crystals, Phys. Rev. Lett. 76 (1996) 3594–3597, https://doi.org/10.1103/PhysRevLett.76.3594.
[27] T. Trusty, S. Xu, I.J. Beyerlein, Atomistic simulations of tungsten nanotubes under uniform tensile loading, J. Appl. Phys. (2019), https://doi.org/10.1063/1.5110167.
[28] S. Xu, S.Z. Chavoshi, Uniaxial deformation of nanotwinned nanotubes in body-centered cubic tungsten, Curr. Appl Phys. 18 (2018) 114–121, https://doi.org/10.1016/j.cap.2017.10.003.
[29] J. Hou, X.-S. Kong, C.S. Liu, J. Song, Hydrogen clustering in bcc metals: atomic origin and strong stress anisotropy, Acta Mater. 201 (2020) 23–35, https://doi.org/10.1016/j.actamat.2020.09.048.
[30] R.D. Smirnov, S.I. Krasheninnikov, Stress-induced hydrogen self-trapping in tungsten, Nucl. Fusion. 58 (2018), 126016, https://doi.org/10.1088/1741-4326/aae2c7.
[31] N. Mathew, D. Perez, W. Suk, B.P. Uberuaga, E. Martinez, Interstitial hydrogen enhances the mobility of some grain boundaries in tungsten, Nucl. Fusion. 62 (2022), 086016, https://doi.org/10.1088/1741-4326/ac70e9.
[32] L.-F. Wang, X. Shu, G.-H. Lu, F. Gao, Embedded-atom method potential for modeling hydrogen and hydrogen-defect interaction in tungsten, J. Phys. Condens. Matter 29 (2017), 435401, https://doi.org/10.1088/1361-648x/aa86bd.
[33] L. Gao, A. Manhard, W. Jacob, U. von Toussaint, M. Balden, K. Schmid, High-flux hydrogen irradiation-induced cracking of tungsten reproduced by low-flux plasma exposure, Nucl. Fusion. 59 (2019), 056023, https://doi.org/10.1088/1741-4326/ab0915.
[34] D.H. Tsai, The virial theorem and stress calculation in molecular dynamics, J. Chem. Phys. 70 (1979) 1375–1382, https://doi.org/10.1063/1.437577.
[35] A.P. Thompson, H.M. Aktulga, R. Berger, D.S. Bolintineanu, W.M. Brown, P. S. Crozier, P.J. in 't Veld, A. Kohlmeyer, S.G. Moore, T.D. Nguyen, R. Shan, M. J. Stevens, J. Tranchida, C. Trott, S.J. Plimpton, LAMMPS - a flexible simulation tool for particle-based materials modeling at the atomic, meso, and continuum scales, Comput. Phys. Commun. 271 (2022), 108171, https://doi.org/10.1016/j.cpc.2021.108171.
[36] A. Stukowski, Visualization and analysis of atomistic simulation data with OVITO–the open visualization tool, Model. Simul. Mater. Sci. Eng. 18 (2009), 015012, https://doi.org/10.1088/0965-0393/18/1/015012.
[37] M.-C. Marinica, L. Ventelon, M.R. Gilbert, L. Proville, S.L. Dudarev, J. Marian, G. Bencteux, F. Willaime, Interatomic potentials for modelling radiation defects and dislocations in tungsten, J. Phys. Condens. Matter 25 (2013), 395502, https://doi.org/10.1088/0953-8984/25/39/395502.
[38] Z.A. Piazza, M. Ajmalghan, Y. Ferro, R.D. Kolasinski, Saturation of tungsten surfaces with hydrogen: a density functional theory study complemented by low energy ion scattering and direct recoil spectroscopy data, Acta Mater. 145 (2018) 388–398, https://doi.org/10.1016/j.actamat.2017.12.029.
[39] A.A. Griffith VI, The phenomena of rupture and flow in solids, Philos. Trans. R. Soc. Lond. Ser. A, Contain. Pap. Math. Phys. Character 221 (1921) 163–198, https://doi.org/10.1098/rsta.1921.0006.
[40] T. Suzudo, K. Ebihara, T. Tsuru, H. Mori, Cleavages along {110} in bcc iron emit dislocations from the curved crack fronts, Sci. Rep. 12 (2022) 19701, https://doi.org/10.1038/s41598-022-24357-5.
[41] B. Ma, Q. Rao, Y. He, Effect of crystal orientation on tensile mechanical properties of single-crystal tungsten nanowire, Trans. Nonferrous Metals Soc. China 24 (2014) 2904–2910, https://doi.org/10.1016/S1003-6326(14)63425-7.
[42] A. Pineau, A.A. Benzerga, T. Pardoen, Failure of metals I: brittle and ductile fracture, Acta Mater. 107 (2016) 424–483, https://doi.org/10.1016/j.actamat.2015.12.034.
[43] W.R. Tyson, R.A. Ayres, D.F. Stein, Anisotropy of cleavage in B.C.C. transition metals, Acta Metall. 21 (1973) 621–627, https://doi.org/10.1016/0001-6160(73)90071-0.
[44] A. Almasri, G. Voyiadjis, Physically based constitutive model for body centered cubic metals with applications to iron, J. Eng. Mech.-ASCE 134 (2008), https://doi.org/10.1061/(ASCE)0733-9399(2008)134:7(521).
[45] G. Testa, N. Bonora, A. Ruggiero, G. Iannitti, Flow stress of bcc metals over a wide range of temperature and strain rates, in: 2020. https://doi.org/10.3390/met10010120.
[46] K. Maruyama, 8 - Fundamental aspects of creep deformation and deformation mechanism map, in: F. Abe, T.-U. Kern, R. Viswanathan (Eds.), Creep-Resistant Steels, Woodhead Publishing, 2008, pp. 265–278, https://doi.org/10.1533/9781845694012.2.265.
[47] D. Cereceda, M. Diehl, F. Roters, D. Raabe, J.M. Perlado, J. Marian, Unraveling the temperature dependence of the yield strength in single-crystal tungsten using atomistically-informed crystal plasticity calculations, Int. J. Plast. 78 (2016) 242–265, https://doi.org/10.1016/j.ijplas.2015.09.002.
[48] T. Hasebe, Multiscale crystal plasticity modeling based on field theory, Comput. Model. Eng. Sci. 11 (2006) 145–156, https://doi.org/10.3970/cmes.2006.011.145.
[49] H. Fan, Q. Wang, J.A. El-Awady, D. Raabe, M. Zaiser, Strain rate dependency of dislocation plasticity, Nat. Commun. 12 (2021) 1845, https://doi.org/10.1038/s41467-021-21939-1.
[50] W.P. Wu, Z.Z. Yao, Influence of a strain rate and temperature on the crack tip stress and microstructure evolution of monocrystalline nickel: a molecular dynamics simulation, Strength Mater. 46 (2014) 164–171, https://doi.org/10.1007/s11223-014-9531-0.
[51] E.J. Song, H.K.D.H. Bhadeshia, D.-W. Suh, Effect of hydrogen on the surface energy of ferrite and austenite, Corros. Sci. 77 (2013) 379–384, https://doi.org/10.1016/j.corsci.2013.07.043.
[52] X. Xing, M. Yu, W. Chen, H. Zhang, Atomistic simulation of hydrogen-assisted ductile-to-brittle transition in α-iron, Comput. Mater. Sci. 127 (2017) 211–221, https://doi.org/10.1016/j.commatsci.2016.10.033.
[53] T.D. Lee, T. Goldenberg, J.P. Hirth, Effect of hydrogen on fracture of U-notched bend specimens of spheroidized AISI 1095 steel, Metall. Trans. A 10 (1979) 199–208, https://doi.org/10.1007/BF02817629.
[54] R.A. Oriani, P.H. Josephic, Hydrogen-enhanced nucleation of microcavities in aisi 1045 steel, Scr. Metall. 13 (1979) 469–471, https://doi.org/10.1016/0036-9748(79)90071-1.
[55] P. Grigorev, D. Terentyev, G. Bonny, E.E. Zhurkin, G.V. Oost, J.-M. Noterdaeme, Interaction of hydrogen with dislocations in tungsten: an atomistic study, J. Nucl. Mater. 465 (2015) 364–372, https://doi.org/10.1016/j.jnucmat.2015.06.013.
[56] J. Song, W.A. Curtin, Atomic mechanism and prediction of hydrogen embrittlement in iron, Nat. Mater. 12 (2013) 145–151, https://doi.org/10.1038/nmat3479.
[57] T. Depover, E. Wallaert, K. Verbeken, On the synergy of diffusible hydrogen content and hydrogen diffusivity in the mechanical degradation of laboratory cast Fe-C alloys, Mater. Sci. Eng. 664 (2016) 195–205, https://doi.org/10.1016/j.msea.2016.03.107.
[58] R. Yamane, R. Tokiwa, A. Kaneko, T. Takimoto, T. Adachi, H. Tsuchiya, A. Tonegawa, H.T. Uchida, Effect of hydrogen solution on the Young's modulus of rolled tungsten, in: ACTUATOR; International Conference and Exhibition on New Actuator Systems and Applications 2021, 2021, pp. 1–4.
[59] C. Zener, J.H. Hollomon, Effect of strain rate upon plastic flow of steel, J. Appl. Phys. 15 (1944) 22–32, https://doi.org/10.1063/1.1707363.